Modeling Isotope Separation in Electrochemical Lithium Deposition

View the article online for updates and enhancements.

Modeling Isotope Separation in Electrochemical Lithium Deposition

Joseph Wild, Peiyu Wang, Tianwei Jin, and Yuan Yang[z]

Program of Materials Science and Engineering, Department of Applied Physics and Applied Mathematics, Columbia University, New York, NY 10027, United States of America

Naturally occurring Li consists of two stable isotopes, ^{6}Li with an abundance of about 7.5%, and ^{7}Li making up the remainder with 92.5%. The development of a ^{6}Li enrichment technique, in terms of technical reliability and environmental safety to reach ^{6}Li future requirements, represents a key step in the roadmap for nuclear fusion energy supply worldwide. This paper uses finite element analysis-based models to simulate electrochemical Li isotope separation, which is an attractive method in terms of simplicity, safety, and scalability. In the model, we quantitatively analyze how different electrochemical factors including thermodynamics, charge-transfer kinetics, and diffusivities affect the separation process (separation factor), together with cell parameters, such as cell length and current density. The maximum separation factor of 1.128 could be obtained with the cell under the optimal thermodynamic, kinetic, and diffusive conditions, which is among the highest separation factors ever reported. These results will assist in designing the actual isotope separation setup with large separation factor and appropriate timing for sample collection.
© 2022 The Electrochemical Society ("ECS"). Published on behalf of ECS by IOP Publishing Limited. [DOI: 10.1149/1945-7111/ac5854]

Nuclear fusion is considered as the ultimate energy source as it is clean and of extremely high energy density. Among various fusion reactions, the deuterium-tritium (D–T) collision reaction (reaction 1) is popular since its reaction rate peaks at a high value and a low temperature ($\sim$70 keV).[1] ^{6}Li is widely used to produce tritium by neutron bombardment (reaction 2), which is the most promising source for tritium breeding in fusion.[2] On the other hand, ^{7}Li with high purity is attractive for the application of pressurized water reactors in nuclear fission.[3] Both applications require generating these isotopes with high purity. However, ^{6}Li and ^{7}Li have natural abundances of $\sim$7.5% and $\sim$92.5%, respectively. Hence, it is necessary to separate lithium isotopes before they can be used for these important energy applications.

$$D + T \rightarrow {}^4_2He + n + 17.6 \, MeV \qquad [1]$$

$$^6Li + n \rightarrow T + {}^4_2He + 4.8 \, MeV \qquad [2]$$
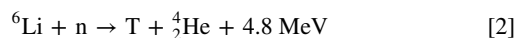
Historically, the Column Exchange (COLEX) process was used to separate ^{6}Li and ^{7}Li, which is based on the ion exchange between Li$_x$Hg alloy and LiOH aqueous solution.[4] However, due to the toxicity of mercury and consequent environmental concerns, many other methods have been explored, such as chemical exchange,[5] ion exchange membrane,[6] chromatography,[7] laser extraction,[8] and electrochemical separation.[9] The electrochemical separation of lithium isotopes is of growing interest and shows potential for achieving a reasonable separation factor. The single stage separation factor, or selectivity, α, is defined as the isotope ratio in two chemically immiscible phases as given in Eq. 3. In electrochemical separation, the as-deposited solid lithium is considered as the first phase, and the lithium ions in the electrolyte[9] or the initial lithium in the anode[10] are the second phase, depending on the nature of the separation.

$$\alpha = \frac{([^6Li]/[^7Li])_1}{([^6Li]/[^7Li])_2} \qquad [3]$$

Electrochemical lithium separation in liquid and gel electrolytes has been studied in the past several decades. For example, Zhang et al.[11] reported that ^{7}Li can be enriched with a selectivity of 1.054 by the application of an electric field in the 1-Butyl-3-

methylimidazolium dicyanamide ([BMIM][DCA]) ionic liquid electrolyte with LiBr as the solute. Moreover, Li isotope separation can be achieved by electrodeposition or by reacting with different electrode materials. For instance, Black et al.[10] reported that ^{6}Li was preferentially plated on a nickel current collector from 1 M LiClO$_4$ in propylene carbonate (PC), with the selectivity ranging from 1.022 to 1.031 as a function of the overpotential due to the electrochemical isotope effect. Hashikawa et al.[12] also reported that ^{6}Li preferentially intercalates into a graphite electrode from lithium naphthalene in 1-methoxybutane with a selectivity of 1.023. However, little work has been done on understanding how different thermodynamic, kinetic, and cell parameters affect the electrochemical lithium isotope separation quantitatively.

In this paper, we use COMSOL Multiphysics to simulate the effects of several key parameters, such as the equilibrium electrode potential, charge transfer kinetics, and ionic diffusivity in the electrolyte, on isotope separation of as-deposited lithium in a symmetric Li|electrolyte|Li cell. The effects of cell parameters such as cell length and current density are also analyzed to explore the optimal conditions for electrochemical isotope separation in terms of separation factor and time to steady state. After understanding individual factors, we combined the optimal conditions together, which can potentially lead to a high selectivity of 1.128, larger than the $\sim$1.05 in the standard COLEX process. This study also investigates parameters for scalable electrochemical lithium isotope separation by balancing the separation factor and the separation time through varying the cell length. These simulation results provide a guide to designing electrochemical separation strategies with large selectivity.

Model Description

Geometry and initial conditions.—The geometry and settings of the model are based on a symmetric cell for electrodeposition, as shown in Fig. 1. Two lithium metal electrodes were separated by a liquid electrolyte or a solid electrolyte horizontally. The left boundary was set as the cathode (lithium deposition), and the right boundary was set as the anode (lithium stripping). The cross-sectional area of the electrodes was 1 cm^2, and the length of the electrolyte domain was set to 1 mm unless other lengths are mentioned. The temperature was 298.15 K, and the total exchange current density at each electrode was 1 mA cm^{-2}. Initially, isotope fractions in the lithium electrodes and electrolytes were the same as their natural abundance ratio r_0 (= 7.5%/92.5% = 0.0811). This is equivalent to 0.075 M ^{6}Li$^+$, 0.925 M ^{7}Li$^+$, and 1 M anion in the
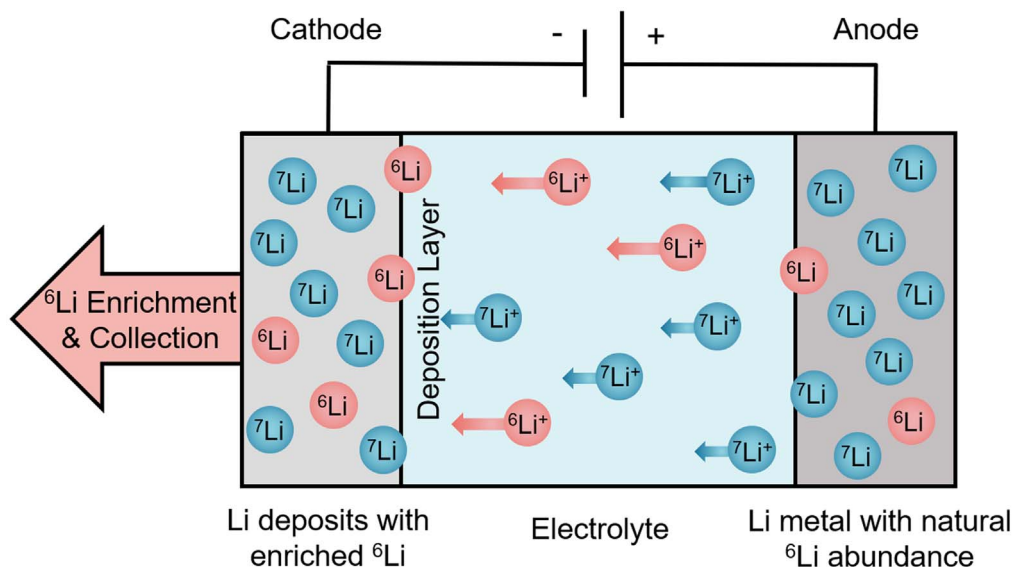
[z]E-mail: yy2664@columbia.edu

Figure 1. The schematic diagram for electrochemical ^{6}Li enrichment. After applying a constant current density to the cell, solid lithium is electrodeposited onto the cathode substrate surface (left) with a ratio of [^{6}Li]/[^{7}Li] greater than the original natural abundance of 0.0811 due to several isotope dependent effects such as thermodynamics, kinetics, and diffusivity, which represents that the ^{6}Li in the deposition layer is successfully enriched.

liquid electrolyte, and 0.375 M ^{6}Li$^+$, 4.625 M ^{7}Li$^+$, and 5 M effectively immobile anions in the solid electrolyte. In addition, the anode is assumed infinitely thick and hence the [^{6}Li]/[^{7}Li] ratio is always r_0 at its surface.

Governing equations.—The Nernst-Planck equation under the diluted limit Eq. 4 with the Nernst-Einstein relation Eq. 5 is used as the governing equation for mass transfer in the electrolyte

$$N_i = -D_i \nabla C_i - z_i u_i F C_i \nabla \phi \qquad [4]$$

$$u_i = \frac{D_i}{RT} \qquad [5]$$

where N_i, D_i, C_i, z_i, and u_i are the flux density, diffusivity, concentration, charge number, and mobility of species i, respectively, F is the Faraday constant, and Φ is the electrolyte potential. R is the universal gas constant. T is the temperature. In the liquid electrolyte, D_{anion} is of the same order as the cations at 10^{-10} m^2 s^{-1}. In the solid electrolyte, D_{anion} is set to 5×10^{-19} m^2 s^{-1}, 10^7 smaller than the diffusivity of the cations at 5×10^{-12} m^2 s^{-1}, so that they are effectively immobile.

The materials balance Eq. 6 is

$$\frac{\partial C_i}{\partial t} + \nabla \cdot N_i = 0 \qquad [6]$$

Electroneutrality is applied to the liquid electrolyte Eq. 7

$$\sum_i z_i C_i = C_{7_{Li}} + C_{6_{Li}} - C_{anion} = 0 \qquad [7]$$

In the case of solid-state electrolyte, the Poisson charge conservation model Eqs. 8 and 9 is used instead of electroneutrality:

$$\nabla \cdot \boldsymbol{D} = F \sum_i z_i C_i = F(C_{7_{Li}} + C_{6_{Li}} - C_{anion}) \qquad [8]$$

$$D_l = -\varepsilon_0 \varepsilon_r \nabla \phi_l \qquad [9]$$

where $\boldsymbol{D}$ is the electric displacement field in the electrolyte, ε_0 is the vacuum permittivity, and ε_r is the relative permittivity (dielectric constant).

Boundary conditions.—In this study, a constant current density of 3 mA cm^{-2} was applied to the cell unless otherwise stated and the initial boundary electric potentials were set as zero at both ends. The electrode reaction (reaction 10) is as follows:

$$\text{Li}^+(\text{electrolyte}) + \text{e}^- \leftrightarrow \text{Li}(\text{metal}) \qquad [10]$$

The electrode equilibrium potentials for ^{6}Li$^+$/^{6}Li and ^{7}Li$^+$/^{7}Li were governed by their own Nernst Equations at equilibrium, as shown in Eq. 11, and the local current densities were derived from the concentration dependent Butler-Volmer kinetics equations given in Eqs. 12, 13, and 14.

$$E_{eq,i} = E_i^0 - \frac{RT}{F} \ln\left[\frac{C_R^*}{C_O^*}\right] \qquad [11]$$

$$j_{loc,i} = j_{0,i}\left[\tilde{C}_{R,i} \exp\left(\frac{\alpha_a F \eta_i}{RT}\right) - \tilde{C}_{O,i} \exp\left(\frac{-\alpha_c F \eta_i}{RT}\right)\right] \qquad [12]$$

$$j_{0,i} = F k_i (C_{O,i}^*)^{\alpha_a}(C_{R,i}^*)^{\alpha_c} \qquad [13]$$

$$\eta_i = E - E_{eq,i} = [\phi_{ext} - \phi] - E_{eq,i} \qquad [14]$$

$$\alpha = (j_{loc,6}/j_{loc,7})/r_0 \qquad [15]$$

where i is for either ^{6}Li$^+$/^{6}Li or ^{7}Li$^+$/^{7}Li (two separate redox reactions). E_{eq} is the equilibrium potential. E^0 is the formal equilibrium potential at the standard state. C_R and C_O are the surface concentrations of the reduced and oxidized species, respectively. C_R^* and C_O^* are the bulk concentrations of the reduced and oxidized species, respectively. $\tilde{C}_{R,i} = \frac{C_{R,i}}{C_{R,i}^*}$ and $\tilde{C}_{O,i} = \frac{C_{O,i}}{C_{O,i}^*}$ are the normalized concentration of the reduced and the oxidized species, respectively. j_{loc} is the local current density. j_0 is the exchange current density. α_a and α_c are the anodic and cathodic charge transfer coefficient, respectively, which are assumed to both be 0.5 in this manuscript. η is the overpotential, where a positive value corresponds to an oxidation current. E is the electrode potential vs the adjacent reference, Φ_{ext} is the electrode potential with respect to ground, and k is the reaction rate constant for the charge transfer reaction.

The equations above can then be solved to obtain the time-dependent transport behavior in such Li–Li symmetric cells. The time-dependent selectivity, α, is defined as the ratio of ^{6}Li flux over ^{7}Li flux at the cathode, relative to the natural ratio, $r_0 = 0.0811$, in the anode bulk, as given in Eq. 15. This is because the flux represents the isotope deposition ratio onto the cathode surface.

Since the natural abundances in both the electrode and electrolyte are the same, the electrode equilibrium potentials for ^{6}Li$^+$/^{6}Li and ^{7}Li$^+$/^{7}Li are only determined by their formal equilibrium potential at the standard state, so Eq. 11 can be simplified as $E_{eq,i} = E_i^0$.
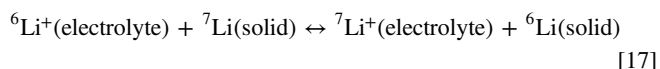
Equation 12 can be further simplified at the anode/electrolyte interface, since $\tilde{C}_{R,i}$ is always 1 as discussed in the 'Geometry and initial conditions' Section. Therefore, at this interface there is Eq. 16 as follows

$$j_{loc,i} = j_{f,i} - j_{r,i} = j_{0,i}\left[\exp\left(\frac{f\eta_i}{2}\right) - \tilde{C}_{O,i}\exp\left(\frac{-f\eta_i}{2}\right)\right] \quad [16]$$

where j_f and j_r are the forward and reverse reaction current densities, respectively, and $f = F/RT = 1/(25.7\text{ mV})$ at T = 298.15 K.

Results and Discussion

Effects of thermodynamic driving force.—Reaction 17 shows the overall reaction of the electrochemical process investigated, and the cell voltage E $= -\Delta G/F = -(\Delta H - T\Delta S)/F$. While isotopes have the same electronic structure (i.e., the same ΔH at T = 0 K), their mass difference results in different vibrational modes and hence differences in heat capacity and entropy.[13] Therefore, the Gibbs free energy of chemicals with different isotopes are different, so that Reaction 17 has a nonzero ΔG. In literature, such differences have been observed in several systems and are the basis of the chemical exchange separation method.[13–15]

$$^6\text{Li}^+(\text{electrolyte}) + {}^7\text{Li}(\text{solid}) \leftrightarrow {}^7\text{Li}^+(\text{electrolyte}) + {}^6\text{Li}(\text{solid})$$
$$[17]$$

In this work, it will not be studied how various electrolytes and solid-electrolyte interphases (SEI) affect ΔG, but it is assumed that $\Delta E^0 = E_{^6\text{Li}^+/^6\text{Li}}^0 - E_{^7\text{Li}^+/^7\text{Li}}^0$ can be nonzero, and then the magnitude of isotope separation it can induce is understood. Various combinations of ΔE_c^0 and ΔE_a^0 are considered, where the subscript c and a indicate cathode and anode, respectively. The different ΔE_c^0 and ΔE_a^0 can be realized by pretreating lithium to form different SEI or by using a membrane to separate two electrolytes in advance so that the two electrodes are in contact with different electrolytes.[11] The steady state behavior is only determined by ΔE_a^0, since this is associated with the anode interface where the lithium is extracted. By mass conservation, the steady state quantity and selectivity of lithium extracted from the anode must be the same as that deposited on the cathode surface. Therefore, only nonzero ΔE_a^0 effects are described here. On the other hand, nonzero ΔE_c^0 mainly determines the initial transient behavior, and is discussed in section S3 in the supporting information.

If $\Delta E_a^0 < 0$ mV, then $\eta_{a,^7Li} < \eta_{a,^6Li}$ from Eq. 14. I.e., if the equilibrium potential for the ^{6}Li reaction at the anode surface is lower, then the relative forward current (oxidation) of ^{6}Li is larger than for ^{7}Li, and the reverse current (reduction) of ^{6}Li$^+$ is smaller than ^{7}Li$^+$. Therefore, the net relative ^{6}Li oxidation rate is higher than for ^{7}Li, leading to its preferential extraction.

The analysis above reflects the simulation results of Fig. 2. Figure 2a shows that the selectivity of as-deposited lithium on the cathode surface, α, depends on both ΔE_a^0 and time for the standard cell (1 mm cell length and 3 mA cm^{-2}), where $E_{a,^7Li}^0$ is set as 0 mV. For $E_{a,^6Li}^0 < 0$ mV, the initial α on the cathode is 1, since there has

not been enough time for the higher proportion of ^{6}Li$^+$ extracted from the anode to diffuse to the cathode surface. However, after around 3 h, a steady state selectivity 1.046 is reached whereby the quantity and selectivity of the deposited lithium is the same as that extracted from the anode surface by mass conservation, which has a slight preference for ^{6}Li due to its lower equilibrium potential. The magnitude of α is exponentially dependent on the difference between $E_{a,^6Li}^0$ and $E_{a,^7Li}^0$ (i.e. ΔE_a^0), however, this is effectively linear for the observed small differences in physical systems.

The simulation results are consistent with analytical derivations. Mathematically, based on Eqs. 13, 15, and 16, α can be expressed as Eq. 18, which represents the ratio of the net reaction for ^{6}Li over the net reaction rate for ^{7}Li, normalized to the natural ratio. The two leading exponential terms represent the rate of forward reactions, while the two trailing exponential terms with their concentration-dependent prefactors represent the reverse reactions. Then, for $\eta_{a,6} > \eta_{a,7}$ (for example $\eta_{a,6} = 30.0$ mV and $\eta_{a,7} = 28.0$ mV at j = 1 mA cm^{-2} as in Fig. S1d (available online at stacks.iop.org/JES/169/032504/mmedia)), the forward reaction term for ^{6}Li dominates and leads to an $\alpha > 1$.

$$\alpha = \frac{1}{r_0}\frac{j_{loc,6}}{j_{loc,7}} = \frac{\left[\exp\left(\frac{f\eta_{a,6}}{2}\right) - \tilde{C}_{O,6}\exp\left(\frac{-f\eta_{a,6}}{2}\right)\right]}{\left[\exp\left(\frac{f\eta_{a,7}}{2}\right) - \tilde{C}_{O,7}\exp\left(\frac{-f\eta_{a,7}}{2}\right)\right]} \quad [18]$$

In addition to the main effect caused by the different equilibrium potentials of the isotope reactions, varying the current density and cell length can influence the behavior of the system and the selectivity of the deposited lithium. Simulation results in Fig. 2b show that lower current densities favor higher steady state selectivities. This is because at high current densities only the forward reaction rate is dominant while the reverse reaction magnitude becomes small (e.g. $j_f = 3.52$ mA cm^{-2} and $J_r = 0.52$ mA cm^{-2} at j = 3 mA cm^{-2}). Or in other words, ρ_a defined in Eq. 19, representing the ratio of the total forward reaction rate to the total reverse reaction rate, becomes larger. Therefore, the high current limit for the extracted lithium from the anode only depends on the reduced activation energy for the oxidation of ^{6}Li, as given by Eq. 20. This gives a selectivity value of 1.040 in the limit of high current for $\Delta E_a^0 = -2$ mV.

$$\rho_a = \frac{\exp\left(\frac{f\eta_{a,6}}{2}\right) + \exp\left(\frac{f\eta_{a,7}}{2}\right)}{\tilde{C}_{O,6}\exp\left(\frac{-f\eta_{a,6}}{2}\right) + \tilde{C}_{O,7}\exp\left(\frac{-f\eta_{a,7}}{2}\right)} \quad [19]$$

$$\alpha = \frac{1}{r_0}\frac{j_{loc,6}}{j_{loc,7}} \approx \frac{\exp\left(\frac{f\eta_{a,6}}{2}\right)}{\exp\left(\frac{f\eta_{a,7}}{2}\right)} = \exp\left(\frac{f \times (E_{a,^7Li}^0 - E_{a,^6Li}^0)}{2}\right) \quad [20]$$

In contrast, at low currents densities, both the forward and reverse reactions are of similar magnitudes, with both approaching the exchange current density in the limit of no current, and therefore $\rho_a = 1$. This allows both reactions to contribute equally to the isotope effect, ultimately resulting in the selectivity given in Eq. 21 in the limit of no current. This gives a selectivity value of 1.081 in the limit of no current for $\Delta E_a^0 = -2$ mV.

$$\alpha = \exp\left(f \times (E_{a,^7Li}^0 - E_{a,^6Li}^0)\right) \quad [21]$$

Simulation results in Fig. 2d show that increasing the cell length can have slight benefits for the steady state selectivity when
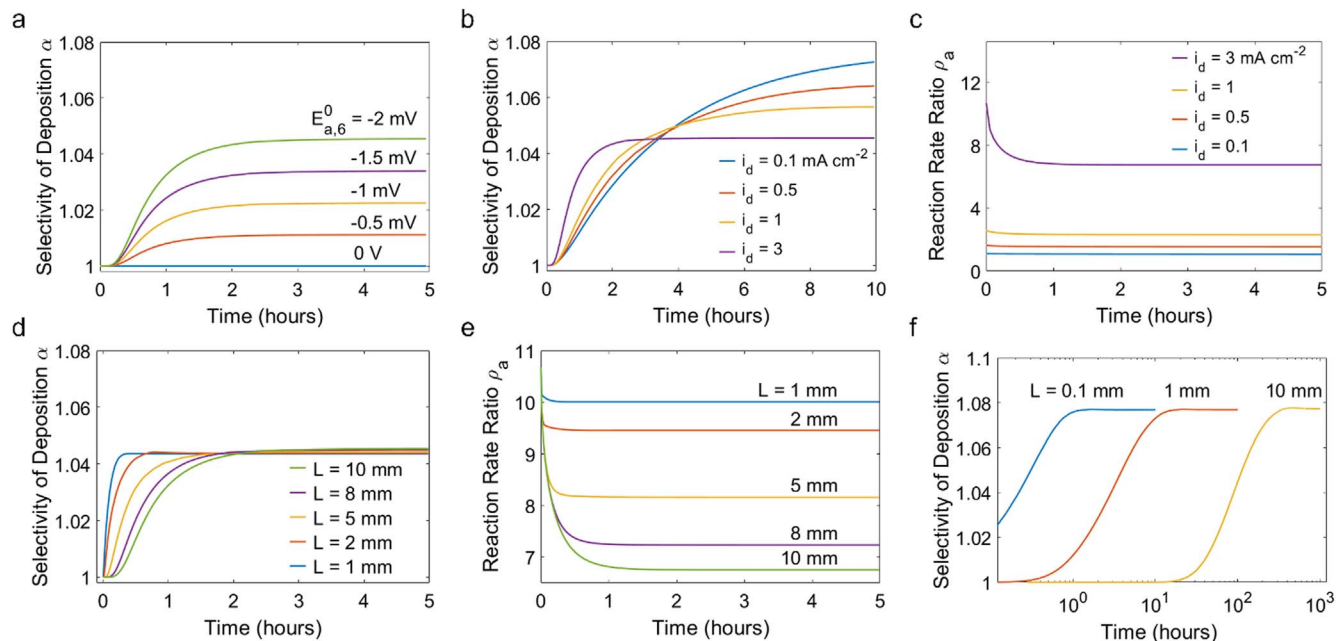
Figure 2. The transient effects of $E_{a,6}^0$ and $E_{a,7}^0$ on lithium isotope separation. In all cases, $E_{c,6}^0 = E_{c,7}^0 = 0$. (a) The dependence of α on $E_{a,6}^0$, with $E_{a,7}^0 = 0$ mV. (b) The dependence of α on the current density with $E_{a,6}^0 = -2$ mV. (c) The dependence of the ratio of the total forward reaction rate to the reverse reaction rate at the anode surface on current. (d) The dependence of α on cell length with $E_{a,6}^0 = -2$ mV. (e) The dependence of the ratio of the forward reaction rate to the reverse reaction rate at the anode surface on length. (f) The transient α for systems with a current density of 0.1 mA cm^{-2}, $E_{a,6}^0 = -2$ mV, and varying lengths.

$\Delta E_a^0 < 0$ mV, however, this comes at the cost of greatly increased times to reach steady state due to increased lengths of diffusion. Increasing the cell length increases the relative surface concentrations, $\tilde{C}_{O,i}$, at the anode for both cation species, owing to the greater length over which a concentration gradient can develop in an electric field. Therefore, this favors the reverse reactions as shown in Fig. 2e by longer cells having a lower reaction rate ratio, ρ_a, due to the greater reverse reaction magnitude. However, the reverse reaction is more difficult for ^{6}Li$^+$ due to its lower equilibrium potential, and

hence this change slightly favors the overall extraction of ^{6}Li compared to ^{7}Li.

By considering the effects of altering both the current density and the cell length, lower current densities and shorter cell lengths are best for achieving good selectivities in reasonable amounts of time. Figure 2f shows simulation results for the selectivity of the deposited lithium with time for a current density of 0.1 mA cm^{-2}, cell lengths of 0.1 mm, 1 mm, and 10 mm, and $E_{a,^6Li}^0 - E_{a,^7Li}^0 = -2$ mV. The 10 mm cell has a slightly higher steady state selectivity of 1.0773
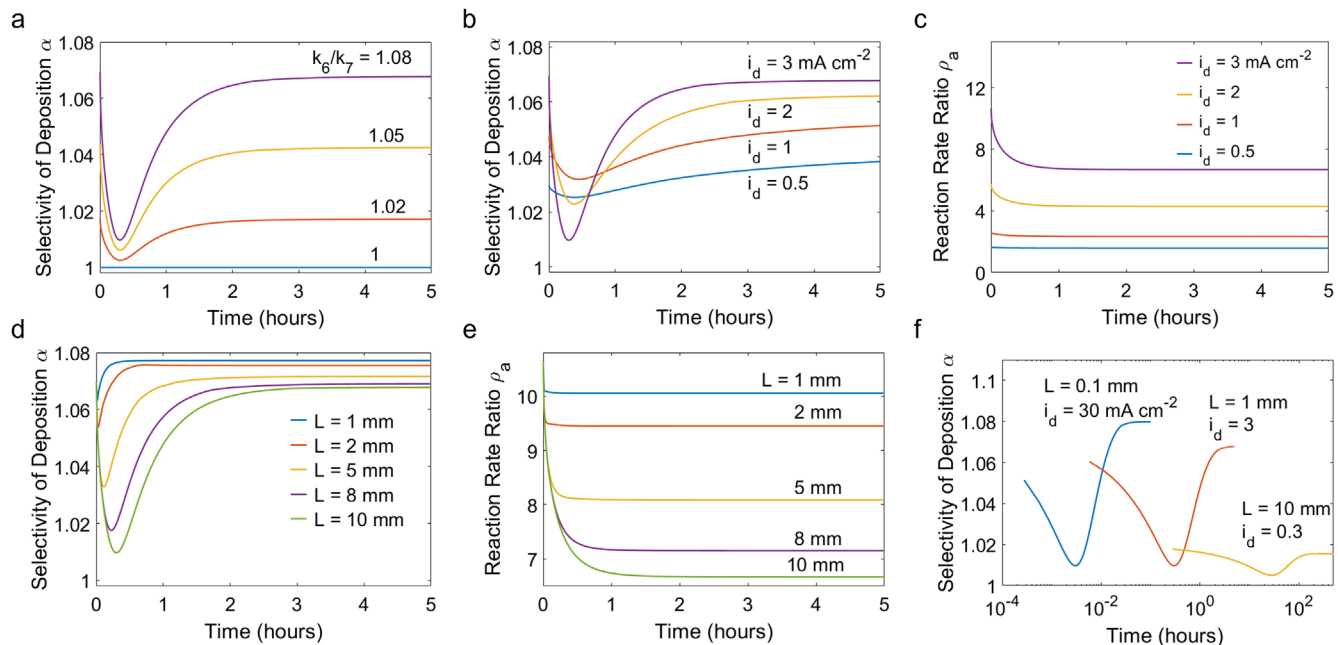

Figure 3. The transient effects of different reaction rate constants at the electrode surfaces on lithium isotope separation. (a) The dependence of α on k_6/k_7. (b/c) The dependence of (b) α and (c) ρ_a on the current density when $k_6/k_7 = 1.08$. (d/e) The dependence of (d) α and (e) ρ_a on cell length when $k_6/k_7 = 1.08$. (f) The transient α for systems with equal steady state electrolyte polarization but with variations in length and current, $k_6/k_7 = 1.08$.

compared to 1.0769 for the 0.1 mm cell but takes around 400 h to reach steady state, compared to around 1 h for the 0.1 mm cell. Therefore, a current density of ∼0.1 mA cm^{-2} and a cell length of ∼0.1 mm is recommended for systems where the isotope effect is driven by thermodynamic differences.

Finally, since f of Eqs. 18, 20, and 21 is inversely proportional to temperature, lower temperatures will result in higher selectivities when there is a thermodynamic driving force for the isotope effect, shown in Fig. S3a, as is consistent with a broad range of experimental data.[16,17]

Effects of charge-transfer kinetics.—The isotope fractionation associated with charge-transfer kinetics stems from the reaction rate constant, k, in Eq. 13, which describes the exchange current densities. Based on the lithium isotope electrochemical effect and Marcus charge-transfer theory, the mass dependence of k follows an inverse square-root relationship (k ∝ $m_{eff}^{-0.5}$), where the effective solute mass is affected by the solvation state of ions (i.e., number of solvent molecules in the solvation complex) of specific electrolyte solutions.[18] Generally, the ratio of k_6/k_7 has a classic upper limit of $(6.015/7.016)^{-0.5} = 1.080$, and so the considered k_6/k_7 are 1, 1.03, 1.05, and 1.08 in this section. It should be noted that for an assumed reaction rate constant ratio, this ratio is applied to both the anode and the cathode in Eq. 13.

The simulation results are shown in Fig. 3, with Fig. 3a showing the dependence of the selectivity as a function of k_6/k_7 and time for the standard 1 mm, 3 mA cm^{-2} cell. For $k_6/k_7 > 1$, for example 1.08, the selectivity of the deposited lithium initially decreases rapidly from 1.08 to a minimum of 1.010 after 18 min, before rising to a steady state value of 1.068 after around 3 h. Physically, the initial sharp decrease of α is because the larger k_6 leads to $j_{loc,6}/j_{loc,7} > r_0$, and thus $^6Li^+$ is depleted more rapidly at the cathode surface, which reduces $[^6Li^+]/[^7Li^+]$, $j_{loc,6}/j_{loc,7}$, and consequently α. For example, after 18 min when α reaches its minimum, $[^6Li^+]/[^7Li^+]$ near the cathode surface is 0.0761, or 6.2% lower than the equilibrium value of 0.0811. This value then increases towards the steady state value as the greater proportion of ^6Li which is removed from the anode begins to diffuse through the electrolyte.

At steady state, α must again be determined by the relative proportion of $^6Li/^7Li$ which is removed from the anode. Mathematically, the resulting expression for this is given in Eq. 22, where the differences in k for each isotope now influence their exchange current densities, $j_{0,i}$, leading to the k_6/k_7 prefactor term, while thermodynamic differences are no longer considered so that $\eta_{a,i}$ are represented as η for both species. This k_6/k_7 prefactor term is the upper limit of the steady state selectivity in this case, and is reached when the forward reaction rates ($\exp(f\eta/2)$) dominate over the reverse reaction rates ($\tilde{C}_{O,i}(\exp(-f\eta/2))$), and hence when ρ_a is high. Therefore, the overall isotope effect is driven by the faster forward reaction rate for ^6Li due to the higher k_6, but is weakened by the also-faster reverse rate for $^6Li^+$. Further quantitative figures and examples are given in section S4 of the supplementary information.

$$\alpha = \frac{1}{r_0}\frac{j_{loc,6}}{j_{loc,7}} = \frac{k_6\left[\exp\left(\frac{f\eta}{2}\right) - \tilde{C}_{O,6}\exp\left(\frac{-f\eta}{2}\right)\right]}{k_7\left[\exp\left(\frac{f\eta}{2}\right) - \tilde{C}_{O,7}\exp\left(\frac{-f\eta}{2}\right)\right]}$$
$$= \frac{k_6}{k_7}\frac{[\exp(f\eta) - \tilde{C}_{O,6}]}{[\exp(f\eta) - \tilde{C}_{O,7}]} \qquad [22]$$

As before, varying the current density and cell length can significantly affect the behavior of the overall system and the isotope effect to the advantage of practical applications. Simulation results in Fig. 3b show that greater current densities favor higher steady state selectivities. This is because increasing the current density increases ρ_a, as shown in Fig. 3c and explained by

Eq. 22; as the current density becomes large, the two leading exponential terms which represent the forward reaction rates begin to dominate, and hence the overall selectivity tends towards the upper limit of the ratio of the reaction rate constants. For example, at a low current density of 0.5 mA cm^{-2}, the overall forward reaction rate is 1.340 mA cm^{-2}, while the reverse reaction rate is 0.840 mA cm^{-2}, leading to a low reaction rate ratio of 1.595 and a selectivity of 1.040. In contrast, for a high current density of 3 mA cm^{-2}, the overall forward reaction rate is 3.491 mA cm^{-2}, while the reverse reaction rate is 0.491 mA cm^{-2}, leading to a high reaction rate ratio of 7.110 and a selectivity of 1.068.

Simulation results in Fig. 3d also show that varying the cell length can have a dramatic effect on α, with shorter cell lengths being beneficial in all cases. Decreasing the cell length reduces the space over which a concentration gradient can develop throughout the electrolyte. Therefore, a shorter cell length again leads to less polarized lithium ions at the anode surface, and hence a lower local concentration which is what drives the reverse reaction. For example, for a current density of 3 mA cm^{-2}, the total [Li$^+$] at the anode surface at steady state is 1.078 M for a 100 μm cell length, but is 1.777 M for a 1 mm cell length. Since the rate of the reverse reaction at the anode is proportional to the surface concentration, a longer cell length then leads to a great magnitude of the reverse reaction, leading to a lower ρ_a as shown in Fig. 3e, which then suppresses the isotope effect. Using the same example as above, the forward and reverse reaction rates are 3.308 mA cm^{-2} and 0.308 mA cm^{-2}, respectively, for the 100 μm cell, and are 3.513 mA cm^{-2} and 0.513 mA cm^{-2}, respectively, for the 1 mm cell. The greater reaction rate ratio for the shorter cell of 10.1 compared to 6.7 for longer cell then leads to its higher selectivity as the forward reaction is more dominant, with an α of 1.077 compared to 1.068.

Across all system variables, greater current densities and shorter cell lengths always favor higher steady state selectivities while also reducing the time to reach steady state, as shown in Fig. 3f. Therefore, it is recommended that a short cell length of ∼100 μm and a high current density of ∼30 mA cm^{-2} be used for systems where the isotope effect is predominantly due to differing reaction rate constants. It can be noted that such high current densities may generate significant heat, which may increase the cell temperature and reduce the separation factor. However, this can be addressed by using a cooling bath to keep the cell temperature at a constant.

Effects of diffusivity in liquid electrolytes.—Ionic transport in the electrolyte plays an important role in electrochemical isotope separation. The isotope diffusivities may be different due to their different masses. Past studies have shown that the diffusivities of lithium ions are inversely related to their isotopic mass (D ∝ $m^{-\beta}$ with $0 \leqslant \beta < 0.2$) in simple fluids and molten solids.[19] Moreover, the mass dependence of D is greatest for solutes whose motions are the most weakly coupled with the solvent molecules.[11] For example, D_6/D_7 is only 1.0023 in water ($\beta \sim 0.015$),[19] whereas the largest D_6/D_7 reported in a liquid electrolyte is 1.0337 in molten silicates ($\beta \sim 0.215$).[20] In this section, the range of considered D_6/D_7 is 1 to 1.03 in liquid electrolytes, since this is the range achieved in literature.[19]

Simulation results in Fig. 4a shows that the selectivity of as-deposited lithium on the cathode surface depends on both D_6/D_7 and time. If $D_6/D_7 = 1$, then the deposited lithium shows no departure from the natural ratio, which is consistent with expectation. When $D_6/D_7 > 1$, for example 1.03, the selectivity rises to a maximum of 1.022 after 25 min before settling down to a steady-state value of 1.004 after around 3 h. The initial transient response arises from the increased diffusivity of $^6Li^+$ in the electrolyte; both isotopes are initially consumed in their natural ratio at the cathode surface, however, $^6Li^+$ can then diffuse more readily through the electrolyte to replenish this deposited lithium, hence increasing the relative proportion of [$^6Li^+$] at the cathode surface ($\tilde{C}_{O,6} > \tilde{C}_{O,7}$). As the second term in Eq. 12 (reverse reaction) dominates j_{loc} in lithium
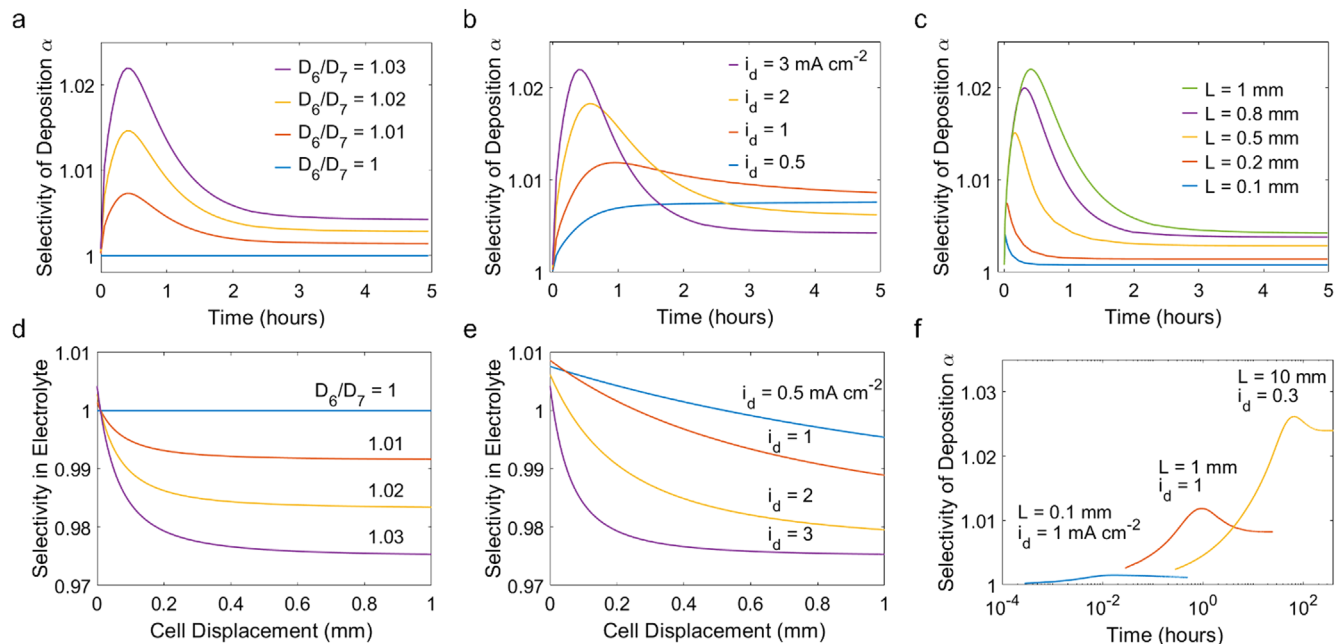
Figure 4. The effects of different isotope diffusivities in the electrolyte on lithium isotope separation. (a)–(c) The temporal dependence of α on (a) D_6/D_7, (b) current density with $D_6/D_7 = 1.03$, (c) cell length with $D_6/D_7 = 1.03$. (d/e) $[^6Li^+]/[^7Li^+]/r_0$ throughout the electrolyte as a function of (d) D_6/D_7 at steady state, (e) current density at steady state, and (f) the transient α for systems with different cell lengths and optimized current density for the steady state selectivity with $D_6/D_7 = 1.03$.

deposition (η is negative), the higher $\tilde{C}_{O,6}$ leads to a higher relative rate of deposition of $^6Li^+$ ($\alpha > 1$), and the magnitude of this effect is proportional to the diffusivity ratios.

At steady state, the quantity and selectivity of lithium which is deposited on the cathode surface must again be the same as that extracted from the anode by mass conservation. Therefore, the steady state behavior is determined only by the magnitude of the forward and reverse reactions at the anode surface for both isotopes. Mathematically, this can be expressed as Eq. 23.

$$\alpha = \frac{1}{r_0}\frac{j_{loc,6}}{j_{loc,7}} = \frac{\left[\exp\left(\frac{f\eta}{2}\right) - \tilde{C}_{O,6}\exp\left(\frac{-f\eta}{2}\right)\right]}{\left[\exp\left(\frac{f\eta}{2}\right) - \tilde{C}_{O,7}\exp\left(\frac{-f\eta}{2}\right)\right]}$$

$$= \frac{[\exp(f\eta) - \tilde{C}_{O,6}]}{[\exp(f\eta) - \tilde{C}_{O,7}]} \qquad [23]$$

The increased diffusivity of $^6Li^+$ in the electrolyte means that it has a smaller relative steady-state spatial gradient of concentration compared to $^7Li^+$, and therefore $C_{O,6}/C_{O,7}$ at the anode surface is smaller than the natural ratio $r_0 = \frac{C^*_{O,6}}{C^*_{O,7}}$. Figure 4d shows that $C_{O,6}/C_{O,7}/r_0 = 0.992, 0.983,$ and 0.976 for $D_6/D_7 = 1.01, 1.02, 1.03$, respectively, at a cell displacement of 1 mm which is the anode surface. Therefore, $\tilde{C}_{O,6} < \tilde{C}_{O,7}$ at the anode surface and so there is a larger overall tendency for ^6Li to be oxidized to $^6Li^+$, compared to $^7Li^+/^7Li$, resulting in $\alpha > 1$ in Eq. 23. For example, the steady state selectivities are 1.0014, 1.0028, and 1.0043 for $D_6/D_7 = 1.01, 1.02,$ and 1.03, respectively, for the standard cell, as shown in Fig. 4a.

Varying the current density and cell length also influences the two isotope ion concentrations at the anode surface and the rate of reactions, which can therefore be used to influence the timescale and magnitude of this isotope effect.

For example, simulation results in Fig. 4b show that greater current densities result in a greater peak selectivity for the deposited lithium, but that an intermediate current density (~ 1 mA cm^{-2}) can

result in the highest value of the steady state selectivity. This is because at low current densities (<1 mA cm^{-2}) the polarization of lithium ions in the electrolyte is small, and so the difference between $\tilde{C}_{O,6}$ and $\tilde{C}_{O,7}$ is small with both being around 1, and thus α is small. Moreover, with a larger current density, the difference between $\tilde{C}_{O,6}$ and $\tilde{C}_{O,7}$ becomes larger ($\tilde{C}_{O,6}/\tilde{C}_{O,7}$ becomes smaller), and thus α increases. For example, when j increases from 0.1 to 0.5 and 1 mA cm^{-2}, $\tilde{C}_{O,6}/\tilde{C}_{O,7}$ decreases from 0.9997 to 0.9954 and 0.9888 while the selectivity rises. On the other side, when the current density is high, although $\tilde{C}_{O,6}/\tilde{C}_{O,7}$ continues to decrease upon increasing current density (polarization), $\exp(f\eta)$ becomes significantly larger than $\tilde{C}_{O,6}$ and $\tilde{C}_{O,7}$, since it increases exponentially, so that α is not sensitive to the difference between $\tilde{C}_{O,6}$ and $\tilde{C}_{O,7}$. For example, at j = 1, 2, and 3 mA cm^{-2}, $\exp(f\eta)/\tilde{C}_{O,7}$ increases from 2.365 to 4.375 and 6.845. Table SII shows how different terms in Eq. 23 vary with current density quantitatively, which verifies the analysis above.

Altering the cell length at a given current density can also substantially affect the magnitude and timescale of the isotope effect, as shown in Fig. 4c, where a tenfold increase in the cell length can increase the peak and steady state selectivity by over fivefold, but also increases the time to steady state by a factor proportional to the square of the cell length. Increasing the cell length increases the overall polarization of both species in the electrolyte and is therefore similar to the effect of increasing current density in that high polarization makes the difference between $\tilde{C}_{O,6}$ and $\tilde{C}_{O,7}$ larger, and $\tilde{C}_{O,6}/\tilde{C}_{O,7}$ becomes smaller. For example, $\tilde{C}_{O,6}/\tilde{C}_{O,7}$ decreases from 0.9876 to 0.9790 and 0.9753 when the cell length increases from 0.2 to 0.5 and 1 mm. On the other side, as $\exp(f\eta)$ depends weakly on cell length, α in Eq. 23 is solely determined by the change of $\tilde{C}_{O,6}$ and $\tilde{C}_{O,7}$. For instance, $\exp(f\eta)$ is 11.2, 11.6, and 12.3 at cell length of 0.2, 0.5 and 1 mm. Therefore, when the cell length increases, α increases monotonously, as shown in Fig. 4e.

In all cases, the limit of the steady state selectivity is D_6/D_7, with near-limiting current densities being optimal for long cells, and some

intermediate current density being optimal for short cells. In general, longer cell lengths favor better selectivities, while shorter cell lengths favor dramatically faster times to reach steady state, as shown in Fig. 4f. By taking both selectivity and operation time into account, a cell length of $\sim$1–10 mm and a current density of $\sim$0.3–1 mA cm^{-2} is recommended.

Effects of diffusivity in solid electrolytes.—As constrained by the Li$^+$ solvation structure and viscosity of electrolyte solutions, it is difficult to achieve D$_6$/D$_7$ higher than 1.03 in liquid electrolytes. However, the diffusion of Li$^+$ in solid electrolytes is controlled by the jumping frequency, which is inversely proportional to the square root of the ion mass in classic theories.[21,22] Hence D$_6$/D$_7$ can reach $(7.016/6.015)^{1/2} = 1.08$ in theory. Moreover, recent studies show that quantum effects could alter the activation barrier energy for Li$^+$ in crystals in a positive way, hence increasing D$_6$/D$_7$ to 1.12 in certain materials (e.g. lithium lanthanum titanate).[23,24] Therefore, here it is also studied how solid electrolytes with different D$_6$/D$_7$ affect α. A major difference in simulating liquid and solid electrolytes is that liquid is a binary electrolyte where the anion has a diffusivity similar to cations (e.g. 10^{-10} m^2 s^{-1} in this study) and electroneutrality holds. In solid electrolytes, however, it is assumed that the anion has an extremely low diffusivity (5×10^{-19} m^2 s^{-1} here), which is effectively immobile, and the Poisson equation is applied instead of electroneutrality. The range of D$_6$/D$_7$ simulated is 1 to 1.08, within the range of values reported in literature.[23–26]

Similar trends are observed regarding the preferential ^{6}Li plating/ stripping processes for solid electrolytes as they were for liquid electrolytes, as shown in Figs. 5a and 5b, for a 1 mm cell length at 3 mA cm^{-2}. For example, for D$_6$/D$_7$ = 1.08, the selectivity reaches a maximum of 1.076 after 1.7 h, before settling to a steady state value of 1.007 after around 15 h.

Again, the selectivity linearly increases with the ratio D$_6$/D$_7$ and is influenced by variations in the cell length and current density. Simulation results showed that different cell lengths had different optimal current densities to achieve the highest steady state selectivity. These optimal combinations are shown in Fig. 5b for cell lengths of 0.1 mm, 1 mm, and 1 cm, with steady state selectivities of 1.010, 1.042, and 1.071, respectively. Longer cell lengths can lead to even higher selectivities, but at the cost of exceedingly long times to steady state. The primary difference in behavior between the solid and liquid electrolyte cases is the significantly longer timescales required to reach steady state in the solid system due to the requirement of slow solid-state diffusion.

Despite generally long timescales required for solid diffusion, an additional strategy was found to be possible in the solid case whereby high selectivities can be reached in a relatively short period of time through a combination of both a long cell length and a high current density, as shown in Fig. 5c, where a deposited selectivity of 1.080 was reached after 5 h and lasted for 70 h in the 2.5 mA cm^{-2}, 25 mm case. The mechanism of this is solely the increased diffusivity of ^{6}Li$^+$ meaning that it can initially diffuse towards the

cathode at a greater rate than ^{7}Li$^+$, which relies on the lithium which is initially in the solid electrolyte. Once the lithium which has been extracted from the anode has time to fully diffuse through the electrolyte the effect is weakened, eventually leading to the lower steady state selectivity observed. This strategy is not possible for liquid electrolytes because the limiting current density would be breached for the given cell length, and so salt depletion would occur. However, even in the solid case, such long cell lengths would be difficult to fabricate and would have very high resistances, leading to high overpotentials at these currents and the oxidation of the electrolyte at the anode interface.

Maximization of the selectivity.—After studying how different thermodynamic, kinetic, and diffusive parameters affect the electrochemical separation process independently, understanding their combined effect is essential for understanding how to optimize the overall selectivity. Hence, promising values for each condition are chosen as an example, such as $\Delta E_a^0 = -2$ mV, k$_6$/k$_7$ = 1.08, and D$_6$/D$_7$ = 1.05 for both the liquid and solid electrolyte cases and are simulated in Figs. 6a and 6b, respectively, for a 1 mm cell length and a range of current densities.

It can be noted that the final selectivity can be well approximated by the product of the independent thermodynamic, kinetic, and diffusive conditions. For example, for the modeled liquid electrolyte with $\Delta E_a^0 = -2$ mV, k$_6$/k$_7$ = 1.08, D$_6$/D$_7$ = 1.05, and 3 mA cm^{-2} current density, the final selectivity of 1.125 is approximately the product of 1.046, 1.068, and 1.007, which are the selectivities of the respective conditions when the other parameters have no preference between isotopes. This shows that these effects compound on top of one another, and that by optimizing these effects independently the overall isotope effect can be substantial. In this way, very large single stage separation factors can be achieved.

The optimal cell conditions in terms of current density and cell length will generally depend upon which isotope effect is dominant in the given system. However, if there are multiple prominent mechanisms, then the optimal conditions can be found via simulation or experiment. For example, for the two simulated cases shown in Figs. 6a and 6b, an intermediate current density of $\sim$1 mA cm^{-2} gives the highest steady state selectivities of 1.128 and 1.127, respectively. This is because an intermediate current density favors the diffusive isotope effect at this cell length, while higher currents favor the reaction rate constant isotope effect, and lower currents favor the thermodynamic isotope effect, resulting in the overall optimal values observed.

Once the combined contributing isotope effects are understood, combinations of cell lengths and current densities can be optimized to find the best combination of steady state selectivity and time to steady state for practical applications. Apart from the reaction rate constant isotope effect, there is generally a trade-off between steady state selectivity and time to steady state. Simulation results in Fig. 6c show the selectivity of the deposited lithium vs time for the same conditions as in Fig. 6a, but for a range of cell lengths and current densities. The
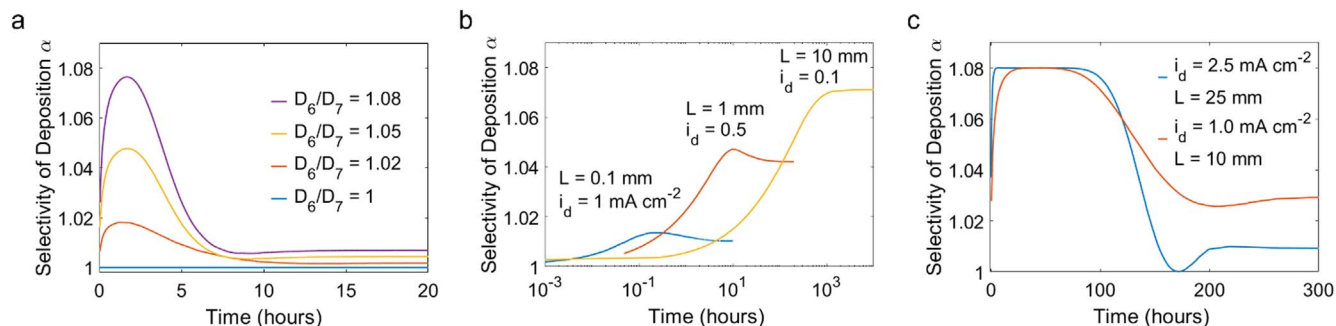

Figure 5. The transient effects of different isotope diffusivities in a solid electrolyte on lithium isotope separation. (a) The dependence of α on D$_6$/D$_7$ in a solid electrolyte. (b) The α for systems with different cell lengths and optimized current density for the steady state selectivity with D$_6$/D$_7$ = 1.08. (c) The α for systems with equal steady state electrolyte polarization but with variations in length and current, D$_6$/D$_7$ = 1.08.
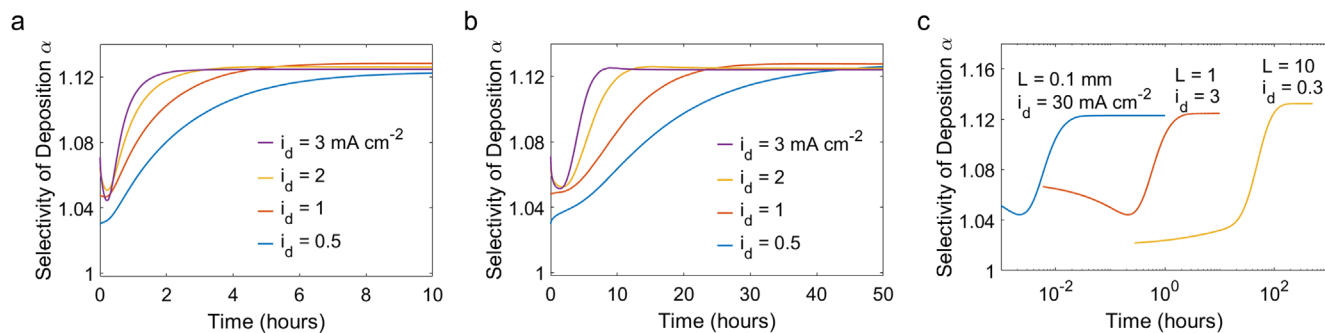
Figure 6. The effects of combining conditions which lead to an isotope effect, for $D_6/D_7 = 1.05$, $k_6/k_7 = 1.08$, $E_{a,6}^0 = -2$ mV. (a) The dependence of α on current and time for the liquid electrolyte case. (b) The dependence of α on current and time for the solid electrolyte case. (c) The transient α for liquid systems with equal steady state electrolyte polarization but with variations in length and current density.

highest selectivity of 1.132 is achieved for the longest cell length of 1 cm, but this system takes hundreds of hours to reach steady state. However, a high current density of 30 mA cm^{-2} and a short cell length of 0.1 mm can still achieved a selectivity of 1.123 while only taking minutes to reach steady state. These forms of results could then be used to guide optimal conditions for multi-stage applications.

Conclusions

In summary, we used finite element analysis-based simulation to investigate the effects of thermodynamics, charge transfer, and transport properties on the electrochemical lithium isotope separation process. The selectivity at the beginning is affected by $E_{c,6}^0 - E_{c,7}^0$ at the cathode, with a lower $E_{c,6}^0$ favoring ^{6}Li$^+$ deposition. α at the steady state is solely determined by $E_{a,6}^0 - E_{a,7}^0$ at the anode, and a lower $E_{a,6}^0$ favors ^{6}Li$^+$ deposition. Moreover, $k_6/k_7 > 1$ and $D_6/D_7 > 1$ also favor ^{6}Li$^+$ deposition and results in $\alpha > 1$. The effects of $E_{a,6}^0 - E_{a,7}^0$ and k_6/k_7 are particularly prominent for liquid electrolytes, while the potential high values of D_6/D_7 are more prominent in solid electrolytes. At the steady state, $E_{a,6}^0 - E_{a,7}^0 = -2$ mV results in an α of 1.046 and $k_6/k_7 = 1.08$ leads to an α of 1.068 for a 1 mm cell length at 3 mA cm^{-2}. Cell length and current density also affect α and the time to reach the steady state, and optimal conditions are discussed.

The combinatory effects of parameters above are also discussed. We find that the effects of thermodynamics, charge transfer, and transport properties can combine multiplicatively to realize higher selectivities. At an optimized condition, a steady state selectivity of 1.128 could be theoretically achieved at $\Delta E_a^0 = -2$ mV, $k_6/k_7 = 1.08$ and $D_6/D_7 = 1.05$. This work demonstrates the initial value of modelling for understanding and guiding complex systems and represents electrochemical lithium isotope separation as a simple, safe, and potentially effective method for achieving the necessary ^{6}Li enrichment for the future fusion energy supply.

ORCID

Yuan Yang https://orcid.org/0000-0003-0264-2640

References

1. V. E. Golant, M. N. Rosenbluth, H. Wobig, S. Nakai, F. Najmabadi, and R. W. Conn, "Plasma physics and controlled nuclear fusion research." *Proc. 13th Int. Conf., Washington, 1990*, **31**, 761 (1991).
2. H. Wang, G. Li, Y. Ge, B. Liu, L. Lin, B. Yang, Y. Li, and P. Jiang, "Research progress and development trend of tritium breeder materials preparation technology for fusion reactors." *Cailiao Daobao/Materials Reports*, **34**, 75 (2020).
3. P. B. Myerscough, *Nuclear Power Generation: Modern Power Station Practice.* (2013).
4. E. A. Symons, "Lithium isotope separation: a review of possible techniques." *Sep. Sci. Technol.*, **20**, 9 (1985).
5. X. Jiang, J. Yongzhong, S. Chenglong, W. Xingquan, Y. Ying, and J. Yan, "Research progress of lithium isotope separation by chemical exchange method." *Huagong Jinzhan/Chemical Industry and Engineering Progress*, **36**, 1 (2017).
6. Z. Zhang, Y. Jia, B. Liu, H. Sun, Y. Jing, Q. Zhang, F. Shao, M. Qi, and Y. Yao, "Extraction and separation of lithium isotopes by using organic liquid film extraction system of crown ether-ionic liquid." *Fusion Eng. Des.*, **161**, 112015 (2020).
7. T. Suzuki, M. Zhang, M. Nomura, T. Tsukahara, and M. Tanaka, "Engineering study on lithium isotope separation by ion exchange chromatography." *Fusion Eng. Des.*, **168**, 112478 (2021).
8. T. Arisawa, Y. Suzuki, Y. Maruyama, and K. Shiba, "Extraction of selectively ionised atomic isotopes from a laser-induced plasma." *J. Phys. D: Appl. Phys.*, **15**, 10 (1982).
9. S. Yanase, T. Oi, and S. Hashikawa, "Observation of lithium isotope effect accompanying electrochemical insertion of lithium into tin." *J. Nucl. Sci. Technol.*, **37**, 10 (2000).
10. J. R. Black, G. Umeda, B. Dunn, W. F. McDonough, and A. Kavner, "Electrochemical isotope effect and lithium isotope separation." *JACS*, **131**, 29 (2009).
11. Z. Zhang, A. Murali, P. K. Sarswat, and M. L. Free, "High-efficiency lithium isotope separation in an electrochemical system with 1-butyl-3-methylimidazolium dicyanamide, 1-ethyl-3-methylimidazolium bis(trifluoromethylsulfonyl)imide, and diethyl carbonate as the solvents." *Sep. Purif. Technol.*, **253**, 117539 (2020).
12. S. Hashikawa, S. Yanase, and T. Oi, "Lithium isotope effect accompanying chemical insertion of lithium into graphite." *Z. Nat.forsch. A*, **57A**, 11 (2002).
13. E. V. Sayre and J. J. Beaver, "Isotope effect in the vibrational frequency spectra and specific heats of sodium hydride and deuteride." *J. Chem. Phys.*, **18**, 584 (1950).
14. M. I. Bagatskii, I. Y. Minchina, V. G. Manzhelii, P. I. Muromtsev, V. S. Parbuzin, and A. I. Krivchikov, "Isotopic effects in heat capacity of solid hydrogens with central intermolecular interactions." *Fiz. Nizk. Temp.*, **16**, 8 (1990).
15. J. Serrano, R. K. Kremer, M. Cardona, G. Siegle, A. H. Romero, and R. Lauck, "Heat capacity of ZnO: isotope effects." *Physical Review B (Condensed Matter and Materials Physics)*, **73**, 9 (2006).
16. Y. Fujii, N. Higuchi, Y. Haruno, M. Nomura, and T. Suzuki, "Temperature dependence of isotope effects in uranium chemical exchange reactions." *J. Nucl. Sci. Technol.*, **43**, 4 (2006).
17. K. Okuyama, I. Okada, and N. Saito, "The isotope effects in the isotope exchange equilibria of lithium in the amalgam-solution system." *J. Inorg. Nucl. Chem.*, **35**, 2883 (1973).
18. R. A. Marcus, "On the theory of electron-transfer reactions. VI. Unified treatment for homogeneous and electrode reactions." *J. Chem. Phys.*, **43**, 2 (1965).
19. F. M. Richter, R. A. Mendybaev, J. N. Christensen, I. D. Hutcheon, R. W. Williams, N. C. Sturchio, and A. D. Beloso, "Kinetic isotopic fractionation during diffusion of ionic species in water." *Geochim. Cosmochim. Acta*, **70**, 277 (2006).
20. F. M. Richter, A. M. Davis, D. J. DePaolo, and E. B. Watson, "Isotope fractionation by chemical diffusion between molten basalt and rhyolite." *Geochim. Cosmochim. Acta*, **67**, 3905 (2003).
21. G. H. Vineyard, "Frequency factors and isotope effects in solid state rate processes." *J. Phys. Chem. Solids*, **3**, 121 (1956).
22. A. D. Le Claire, "Some comments on the mass effect in diffusion." *The Philosophical Magazine: A Journal of Theoretical Experimental and Applied Physics*, **14**, 132 (1966).
23. K. Kobayashi and T. Hoshino, "Numerical investigation for lithium isotope effect in ionic superconductor." *Fusion Eng. Des.*, **136**, 205 (2018).
24. K. Shin-mura, R. Tokuyoshi, H. Tazoe, and K. Sasaki, "Temperature effect on lithium isotope separation by electrodialysis using La0.57Li0.29TiO3 electrolyte." *Fusion Eng. Des.*, **171**, 112577 (2021).
25. S. S. Shioya, T. Nagasaki, T. Matsui, and H. Shigematsu, "Lithium-isotope effect on ionic conductivity of (La0.52Li0.27)0.95Sr0.05TiO2.92." *Solid State Ion. Diffus. React.*, **161**, 1 (2003).
26. S. Kunugi, T. Kyomen, Y. Inaguma, and M. Itoh, "Investigation of isotope effect of lithium ion conductivity in (La, Li)TiO3 single Crystal." *Electrochem. Solid-State Lett.*, **5**, A131 (2002).